



Universidad Autónoma
de Madrid

Biblos-e Archivo
Repositorio Institucional UAM

Repositorio Institucional de la Universidad Autónoma de Madrid
<https://repositorio.uam.es>

Esta es la **versión de autor** del artículo publicado en:
This is an **author produced version** of a paper published in:

Nano Research 13.12 (2020): 3425–3432

DOI: <https://doi.org/10.1007/s12274-020-3030-3>

Copyright: © 2020 Springer

El acceso a la versión del editor puede requerir la suscripción del recurso
Access to the published version may require subscription

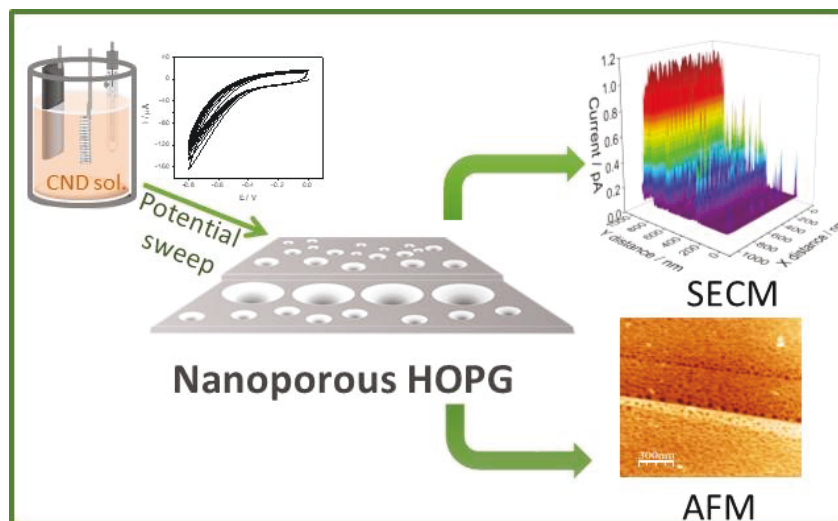
TABLE OF CONTENTS (TOC)

Carbon nanodots: a new precursor to achieve reactive nanoporous HOPG surfaces

C. Gutiérrez-Sánchez ^{1,*}, E. Martínez-Periñán ¹, C. Busó-Rogero ³, M. Revenga-Parra ^{1,2,3}, F. Pariente ^{1,2}, E. Lorenzo ^{1,2,3,*}

¹ Departamento de Química Analítica y Análisis Instrumental and ² Institute for Advanced Research in Chemical Sciences (IAdChem), Universidad Autónoma de Madrid, Campus de Cantoblanco, 28049 Madrid, Spain.

³ IMDEA-Nanoscience. Faraday 9, Campus Cantoblanco-UAM, 28049 Madrid, Spain.



Carbon nanodots: a new precursor to achieve reactive nanoporous HOPG surfaces

C. Gutiérrez-Sánchez ¹ (✉), E. Martínez-Periñán ¹, C. Busó-Rogero ³, M. Revenga-Parra ^{1,2,3}, F. Pariente ^{1,2}, E. Lorenzo ^{1,2,3} (✉)

¹ Departamento de Química Analítica y Análisis Instrumental and ² Institute for Advanced Research in Chemical Sciences (IAdChem), Universidad Autónoma de Madrid, Campus de Cantoblanco, 28049 Madrid, Spain.

³ IMDEA-Nanoscience. Faraday 9, Campus Cantoblanco-UAM, 28049 Madrid, Spain.

© Tsinghua University Press and Springer-Verlag GmbH Germany, part of Springer Nature 2018

Received: day month year / **Revised:** day month year / **Accepted:** day month year (automatically inserted by the publisher)

ABSTRACT

In the present work we develop an electrochemical assisted method to form nanopores on the surface of highly oriented pyrolytic graphite (HOPG), which was accomplished by a simple electrochemical route and a scalable nanomaterial, carbon nanodots, without applying high voltages, high temperatures or toxic reagents. HOPG electrodes are in a solution of N-enriched carbon nanodots in acidic media and the potential scans applied on HOPG lead to the formation of a spatially inhomogeneous porous surface. The diameter of the resulting nanopores can be tuned by controlling the number of electrochemical reduction cycles. The resulting nanoporous surfaces are characterized by atomic force microscopy, Raman spectroscopy, scanning electrochemical microscopy, electrochemical impedance spectroscopy and electrochemistry. These nanoporous HOPG show high capacitance. Hence the potential of these surfaces to the development of energy storage devices is demonstrated.

KEYWORDS

Nanoporous, HOPG, Carbon Nanodots, supercapacitor.

1 Introduction

Nowadays, porous materials are gaining interest because they present a great versatility since they have different fields of application as catalysis [1], separators [2], chemical sensor [3], fuel cell [4], batteries [5] and energy storage as supercapacitor [6]. Another important field of application is medicine and biology [7]. Nanoporous coatings are characterized by having numerous cavities of nanometric size that penetrate in the whole material. They provide the material with a large specific area, better conductivity and an increase in the mass transfer coefficient. In addition, the presence of nanopores in a surface can completely modify its basic properties, since they can make it more reactive and change properties such as texture, density and morphology. However, the preparation of a material with these characteristics requires precision. Researchers have adopted either bottom-up or top-down approaches to prepare nanoporous materials. The first one has been employed to build a surface with nanopores already integrated from the beginning, using nanobubbles as templates of polypyrrol film [8], gold nanoparticles

grown on HOPG [9] and 3D porous materials composed of aggregates of graphene [10]. The second one, to create V-shaped holes by lithography [11].

Highly oriented pyrolytic graphite (HOPG) is an ordered form of a pyrolytic graphite material with a high grade of purity and degree of preferred crystallographic orientation. This feature promotes the wide use of this material in different microscopies. As its surface mainly contains basal planes, it is characterized as a chemically inert material. However, its reactivity changes on increasing the content of edge planes, which makes HOPG a relevant material in nanotechnology applications and nanoscience [12].

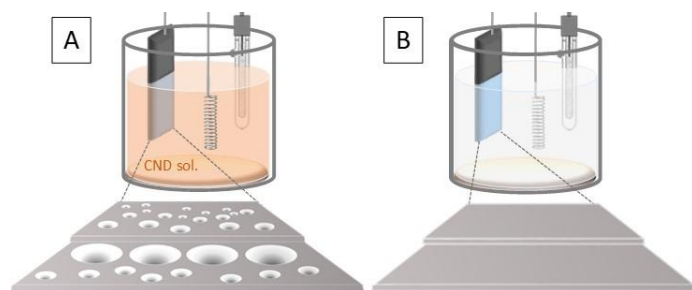
Nanoporous HOPG have been previously prepared using several methods such as AFM bias lithography [13], employing electrochemical etching methodology with microspheres [14], with diazonium salt assisted [15], or a mixture of two aryl diazonium compounds [16]. However, most of the methods employed require severe conditions or are hard to control. Thus, it is of great interest

to explore efficient techniques to prepare nanoporous structures on HOPG surface in large scale.

Carbon is especially attractive for its ability to form bonds with different atoms through different hybrid orbitals sp , sp^2 and sp^3 , that makes this element extremely useful for the construction of nanoporous structures. In addition to traditional active carbons from amorphous carbon, many carbon porous materials have been prepared using carbon-based nanomaterials such carbon nanofibers and carbon nanotubes as the basic building blocks. Therefore, the pursuit of novel carbon nanomaterials as precursors for porous carbons is a deal of great interest. Specifically, carbon nanodots (CND) are emerging carbon-based nanomaterials with a size smaller than 10 nm. They were accidentally discovered during the separation and purification of single walled carbon nanotubes [17]. They have a great structural variety that can be tailored by appropriate selection of the starting materials. For example, functional groups that contain nitrogen can be introduced during synthesis using nitrogen-rich precursors [18]. Due to their excellent properties, they are employed to different applications, but in our knowledge, these nanoparticles have not yet been employed as template to create holes on conductive carbon surfaces, as a simple and smart way to prepare nanoporous carbons. In fact, in spite of nanomaterials have been broadly used to nanostructure small flat surfaces and to increase the specific area, improving other properties such as electronic transfer. As far as we know no report are found concerning the use of nanomaterial for nanostructuring HOPG surfaces.

Supercapacitors are among the most popular types of energy storage devices. They allow for the ultrafast and highly reversible storing and releasing of energy and have a much higher density than electrostatic or electrolytic capacitors. However, the practical applications of supercapacitors are limited by their energy and power densities. Hence, there is a great demand for electrode materials with high capacity. Generally, both the accessible specific surface area and the pore structure determine the performance of electrode materials for supercapacitors. In this regard, porous HOPG would be an optimal material for the development of supercapacitors, since their porous structure allows electrolytes to access to the surface of porous frameworks.

In this work, we demonstrate the ability of CND to generate pores on a HOPG surface in a nanometric scale using a simple, scalable and short preparation electrochemical assisted method. Scheme 1 summarizes this method. HOPG served both as the working electrode and the substrate for nanopores formation. In addition, as proof of concept to prove the utility of this nanoporous carbon it has been applied to the development of an energy storage device, in particular, as supercapacitor.



Scheme 1. Schematic illustration of the strategy followed to obtain nanoporous HOPG from CND solution (A). Control performed in absence of CND (B).

2 Experimental

Chemicals. Urea, fructose, $[\text{Ru}(\text{NH}_3)_6]^{3+}$, $\text{K}_4[\text{Fe}(\text{CN})_6]$ were purchased from Sigma-Aldrich. 37% (w/w) hydrochloric acid was purchased from Scharlau, 95-97 37% (w/w) sulfuric acid was obtained from Fluka. A dialysis membrane tubing cut-off in the range of (0.1-0.5) kDa was provided by Spectrum Laboratories. All solutions were prepared using ultrapure water.

Synthesis of carbon nanodots (CND). The carbon nanodots were synthesized as we previously described [19]. Briefly, fructose and urea precursors were left to react in a microwave oven for 4 min at 750 W. The resulting suspension containing CND was centrifuged, filtered with a nylon mesh of 0.20 mm and dialyzed. The final concentration of CND was 12.7 mg/mL.

Preparation of porous HOPG. HOPG (10x10x2) mm was purchased by Goodfellow. It exfoliates with adhesive tape to obtain a renewed and a flat and exfoliated surface and it is connected to a cooper wire. Then, straightaway the electrode is immersed into an electrochemical cell as working electrode together a platinum wire as counter electrode and a Ag/AgCl as reference electrode in 2.0 mL of a solution containing 12.7 mg/mL of CND in 0.1 M HCl. Consecutive cyclic voltammograms from 0.00 to -0.80 V at 100 mV/s scan rate was recorded as shows Scheme 1. Immediately afterwards electrode is washed with ultrapure water. The number of electrochemical cycles studied were 10, 50 and 100.

Characterization

Electrochemical measurements. Electrochemical experiments were performed with a Metrohm Autolab PGSTAT30 and PGSTAT128N analyzer controlled by GPES 4.9 and NOVA softwares, respectively. Experiments were run in a three-electrode glass cell using a Ag/AgCl reference electrode and a platinum wire counter electrode. The electrochemical measurements for electrode characterization were performed in a home-made Teflon cell where the exposed area of HOPG electrode is controlled (diameter of 4 mm).

Electrochemical impedance spectroscopy (EIS) measurements were recorded using FRA 4.9 software (Metrohm Autolab). Potential applied was 0.21 V using an electrochemical probe, 1.0 mM $\text{K}_4[\text{Fe}(\text{CN})_6]$ in 0.1 M phosphate buffer pH 7.4 containing 0.05 M KCl.

For supercapacitor characterization, it was noted that the charge-discharge curves and cyclic voltammetry for capacitance measurements were obtained using a two-electrode configuration, using two identical HOPG plates, with the same modification process, in any case.

Atomic force microscopy (AFM). Atomic force microscopy (AFM) studies were performed with an Agilent 5500 microscope and Olympus cantilevers (RC800PSA, 200_20 mm) operating in contact mode. All measurements were performed in air.

Scanning electrochemical microscopy (SECM). SECM measurements were carried out with a CH Instruments model 900B scanning electrochemical microscope placed on an antivibration table. A homemade Teflon SECM cell was used. The

electrochemical cell was located on a XYZ positioning stage and the distance between the tip (probe working electrode) and the sample (substrate electrode) was controlled by a stepper motor (coarse approach) combined with a piezoelectric nanopositioning system (fine approach; X, Y, and Z resolution: 1.6 nm; Newport 423 series). All voltammetry and SECM measurements were performed in a grounded Faraday cage using a three-electrode configuration consisting of a Pt wire auxiliary electrode Ag/AgCl saturated reference electrode, and the fabricated Pt UME as the probe electrode. The substrate electrode was highly oriented pyrolytic graphite (HOPG) plates. This electrode has been analysed by SECM before and after modification by generation of the nanopores by the method described before. The tip (Pt UME) used as probe electrode was prepared by the method described in a previous paper, based on a two-step process starting with heating and simultaneously pulling a 25 μm Pt microwire (99.99%, Goodfellow) inserted into a borosilicate glass capillary following by and insulation by step electrochemical polymerization of phenol [20, 21]. The radius of the electrochemical active surface of the UME were calculated from the steady-state limiting current, i_{lim} , (Figure SI 8) assuming a hemispherical geometry via the following Eq. (1):

$$i_{\text{lim}} = 2 \cdot \pi \cdot n \cdot F \cdot D \cdot C^* \cdot r_{\text{app}} \quad (1)$$

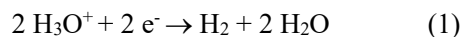
where C^* and D are the bulk concentration of the redox probe (1.0 mM) and diffusion coefficient ($8.43 \times 10^{-6} \text{ cm}^2/\text{s}$) [22] of $[\text{Ru}(\text{NH}_3)_6]^{3+}$ in 0.1 M KCl, respectively; r_{app} is the apparent radius of the exposed section of the tip; n is the number of electrons transferred per molecule (in this case one electron) and F is Faraday's constant. From this equation, we determined that the Pt UME used during the measurement present a r_{app} of 4.0 nm. To avoid any damage to electrodes caused by electrostatic discharge, we handled Pt UME with protection tools [23]. Pt UME were stored and handled in a humidity-controlled box maintaining over 30% relative humidity at 22 °C.

SECM measurements were carried out with all the electrodes immersed in a solution of 1.0 mM $[\text{Ru}(\text{NH}_3)_6]^{3+}$ in 0.1 M KCl. Before surface scanning measurements and with the objective of get closer the tip to the surface of the substrate electrode, an approach curve was made (Figure SI 9). The approach curve is recorded with high accuracy via a slow approach (20 to 1 nm/s) of the tip toward the sample surface. The conditions for the approach were -0.40 V at the tip electrode and open circuit at the substrate electrode vs. Ag/AgCl. This set-up generates an increment of the current of the tip when it is close to the surface of the substrate electrode, because of the feedback mode. So, when the tip current increase over 125 % of the initial current, the approaching stop, and the tip is now enough close to the substrate, which allow it to detect differences on the electrochemical activity of the surface.

Raman Spectroscopy. The Raman measurements were carried out using a confocal Bruker Senterra with a resolution of $3\text{--}5 \text{ cm}^{-1}$, a laser excitation wavelength of 532 nm and a 50x lens Olympus MPlan Achromat (Numerical Aperture=0.75) to focus the laser to the sample.

3 Results and discussion

In order to prepare the nanoporous HOPG surfaces by the electrochemical assisted procedure using CND as precursors, as is depicted in Scheme 1, first nitrogen rich CND are synthesized using urea, as nitrogen source, and fructose, following the procedure previously described [19]. Next, a perfectly exfoliated HOPG plate is immersed, as working electrode, in an electrochemical cell containing a reference and a counter electrode in a solution of the synthesized CND in 0.1 M HCl. Exfoliated HOPG provides an atomically flat and conveniently refreshable surface with reasonable hydrophobicity. It is also an excellent conducting electrode material. Finally, consecutive voltammetric cycles are applied to the HOPG electrode from 0.00 V to -0.80 V at 100 mV/s. No voltammetric peaks, associated to any reduction/oxidation processes other than the hydrogen production according to the reaction (1) are observed in 0.1 M HCl with or without CND (Fig. SI 1).



The presence of CND causes a clear electrocatalytic effect on the reduction of protons according to reaction (1), since both an increase in the current intensity and a decrease in the reduction potential of about +0.15 V is observed (Fig. SI 1). If after several cycles the HOPG electrode is removed from the cell, rinsed with ultrapure water and dried at air, the evolution of the HOPG surface by contact-mode atomic force microscopy (AFM) before and after the treatment shows the differences summarized in Figure 1. Prior the treatment, the HOPG surface is featureless at the magnification used (Fig. 1A). After the electrochemical reduction treatment in presence of CND, a nanoporous HOPG surface is observed (Fig. 1B). In addition, there are considerable differences in the topographic profiles (Fig. 1A and 1B), which is perfectly flat for the exfoliated HOPG before the electrochemical treatment with CND, but shows deepes of 2–4 nm, according to the presence of pores after the treatment. As can be observed in Fig. 1B, the surface is completely perforated with pores of approximately 20 nm in diameter and approximately 2 nm in depth, as can be seen in the profile. It is worth to note that even though the nanopores are randomly distributed on the surface, the nanopores generated in the edge plane are aligned and of greater diameter and depth up to approximately 50 and 4 nm, respectively, that the nanopores generated in the basal plane. This fact can be explained by the greater amount of CND accumulated along the edge plane of HOPG and the higher reactivity of this area [24, 25]. In general, nucleation at pristine basal planes sites tends to occur more slowly than reactions occurring at defect or edges sites. Therefore, based on the above results, under optimal conditions of CND concentration and number of voltammetric cycles, the pores could be made selectively in the edge planes.

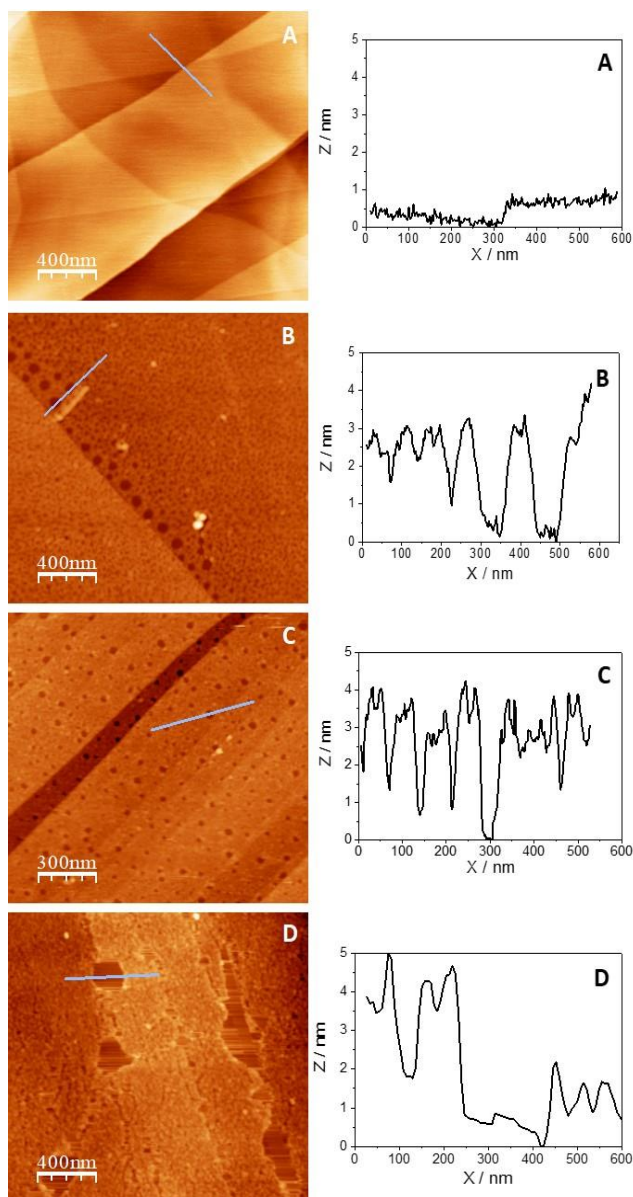


Figure 1. AFM topographic images and their corresponding profiles of exfoliated HOPG prior (A) and after being exposed to electrochemical etching with CND in 0.1 M HCl for 10 (B), 50 (C) and 100 cycles (D).

We have studied the influence of the number of consecutive voltammetric cycles on the nanopore formation and on nanopore size. Figure 1 shows AFM images, and their corresponding profiles, of the resulting nanoporous HOPG electrodes after applying 50 (Fig. 1C) and 100 cycles (Fig. 1D). When the number of voltammetric cycles increased from 10 to 50, as can be observed in Figure 1C, there is a great number of 50 nm pores on the whole surface. The center of maps (Fig. SI 2) associated with the nanopores of Fig. 1A and 1C clearly shows the absence and presence of nanopores on HOPG surfaces before and after the electrochemical etching treatment, respectively. If we make a zoom of the AFM image of Fig. 1C, we can see that the rest of the HOPG surface is also covered with 20 nm and smaller pores (Fig. 2). However, when 100 electrochemical cycles are

performed, the pore size increases up to 200 nm in diameter and it is also appreciated how several pores are grouped, giving rise to those larger pores. The rest of the surface is also covered with small pores (Fig. 1D). If the number of cycles is increased further, the HOPG surface is damaged as shown in Figure SI 3, which could lead to the exfoliation of layers of graphite oxide [26]. These results show that the pore size can be controlled according to the number of voltammetric cycles performed. Furthermore, due to the greater reactivity of surface defects, the distribution of the nanopores can be preferably oriented towards these areas.

When the same electrochemical treatment is carried out in the 0.1 M HCl electrolyte without CND, there is no variation on the HOPG electrode surface, no nanopores are observed (Fig. SI 4). The flat surface obtained proves the role of reduced CND as nanopores precursor.

Although somewhat speculative on our part, we believe that, in addition to requiring CND, hydrogen evolution plays an important role in the nanopore formation mechanism. In the cathodic scan, from 0.00 V to -0.80 V, molecular hydrogen is generated according to the reaction (1), which is catalyzed by/at the CND. Hydrogen generation increases the local pH (by consuming protons), which, in turn, activates the oxygenated functional groups, present at the surface of CND. These activated functional groups would be capable of etching the HOPG surface giving rise to the observed nanopores. In fact, it is well known in the literature that carbon electrodes can be activated by potential cycling in alkaline media. Clearly, the density and size of the nanopores would be expected to increase with time, as was experimentally observed. It should be mentioned that no nanopores formation was observed when potential is cycled from 0 to -0.40 V. This result confirms the important role that hydrogen evolution plays in the nanopore formation process. This fact is in good agreement with previous observations of hydrogen reaction on carbon fabric in aqueous H_2SO_4 [27, 28].

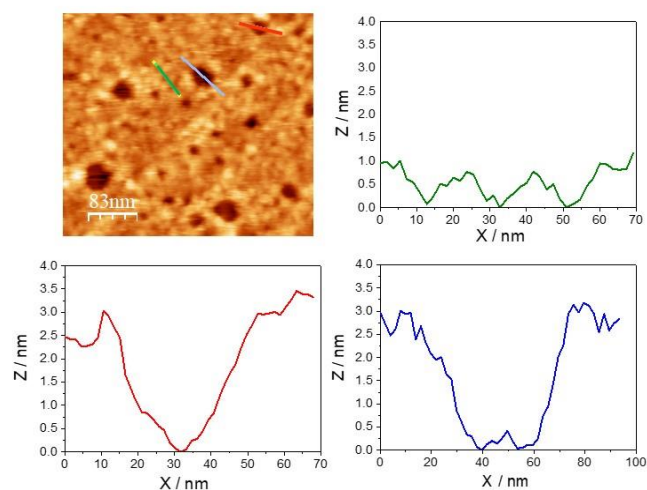


Figure 2. AFM topographic images of nanoporous HOPG (50 cycles) and profiles of nanopores of different sizes.

It has been extensively demonstrated that basal HOPG electrode is less reactive than the edge plane one, since the first is made up of saturated carbon structures. Surface defects play an important role in the electrochemical activity of HOPG electrodes [29], [30]. Thus, one would expect that the presence of nanopores on the HOPG

surface should make it more reactive. To evaluate this possibility, we have studied its electrochemical reactivity by scanning electrochemical microscopy (SECM). This electrochemical technique is an imaging technique capable of providing chemical and topographic information about surfaces immersed in a solution. It is based on moving a small tip electrode very close to a substrate surface. It represents a powerful tool to study the local reactivity in electro(chemical) characterization of surfaces, in particular when nanometer-sized tips are employed.

Here, to improve the spatial resolution scaling-down to the nanoscale, Pt nanoelectrodes with nanometric electroactive area have been fabricated, as described by Lorenzo, E et al. [20, 21] and employed for imaging the distribution of nanopores on the HOPG electrode by using substrate generation/tip collection mode (SG/TC) of SECM. The measurement parameters were obtained employing $[\text{Ru}(\text{NH}_3)_6]^{3+}$ as redox mediator in 0.1 M KCl. $[\text{Ru}(\text{NH}_3)_6]^{2+/3+}$ has a standard potential of $E_0 = -0.17$ V vs. Ag/AgCl, thus, the HOPG substrate electrode was held at a potential of -0.4 V vs. Ag/AgCl to ensure the electrochemical reduction of Ru(III) to Ru(II), while the Pt tip electrode was held at a potential of $E_{\text{tip}} = 0.10$ V vs. Ag/AgCl in order to detect the Ru(II) generated at the HOPG electrode surface. A map of the electrochemical current of the surface associated with the electrochemical activity of the HOPG surface as a function of its morphology and the presence or not of nanopores was obtained.

Once the distance between the Pt nanotip and the substrate surface becomes comparable to the radius of Pt nanotip, the SECM images at constant height and sweeping in X were taken following a parallel line pattern with the lines spaced 1 nm and with the dimensions of 1000×1000 nm at a scanning rate of 200 nm/s. The measurements were also done in the Y-X direction. Images of Fig. 3 show electrochemical reactivity information of exfoliated HOPG (Figure 3A) and nanoporous HOPG electrode (Fig. 3B and 3C) obtained by SECM. As can be seen, the SECM image of a freshly exfoliated HOPG surface, in which no pores have been made, shows two intense signals associated with edge planes (Fig. 3A). The distance between these two intense signals is 400 nm, which corresponds to the distance of areas between folds, according to the AFM images showed above (Fig. 1A) for a similar surface. However, the SECM images of the nanoporous surface are full of peaks randomly distributed on the surface. These arise from the HOPG surface due to the increase in the tip currents as a consequence of the substrate-generated species reacting under diffusion-controlled conditions, when the tip is above the nanopores. The topographic features observed when $[\text{Ru}(\text{NH}_3)_6]^{3+}$ is reduced to $[\text{Ru}(\text{NH}_3)_6]^{2+}$ on the nanoporous HOPG electrode surface, and oxidized back at the tip is indicative that nanopores are the more electrochemical reactive points of the HOPG surface. It can also be observed, that the number of peaks arising from the nanoporous HOPG surface increases as it has been obtained applying more voltammetric cycles (compare Fig. 3B and 3C corresponding to 10 and 50 cycles, respectively). Hence, in agreement with the results obtained by AFM, in general, the higher the number of voltammetric cycles applied, the greater the number

and the size of nanopores produced. These data suggest that the presence of nanopores generates defects, an increase in edge planes in a HOPG surface, that produces an increase in the reactivity.

The spherical shape of an individual nanopore can be achieved in the SECM mapping image as presented in Fig. 3D and Fig. SI 5, where pores with different nanometer sizes (approximately 40 nm

and 20 nm, respectively) are observed. These different size populations are also observed in the AFM images (Fig. 2).

It has previously reported that SECM is employed for determining the catalytic activity of gold [31], platinum [23] nanoparticles and enzymes [21]. In addition, with the results obtained in this work, it is revealed a new application of SECM, the detection of nanometer pores in a HOPG surface.

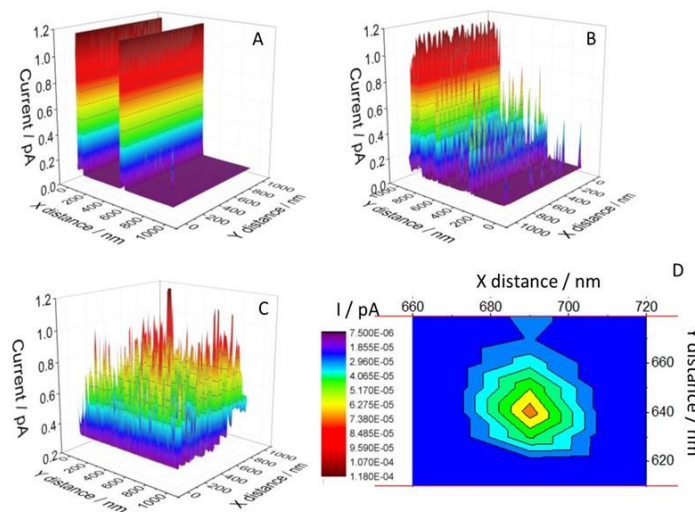


Figure 3. A) SECM image of exfoliated HOPG. B) SECM image of nanoporous HOPG (10 cycles with CND solution). C) SECM image of nanoporous HOPG (50 cycles with CND solution). D) SECM mapping of an individual pore. All measurements were obtained with 1.0 mM $[\text{Ru}(\text{NH}_3)_6]^{3+}$ in 0.1 M KCl at $E_{\text{tip}} = +0.10$ V and $E_{\text{substrate}} = -0.40$ V vs. Ag/AgCl. Pt Nanotip radius = 4.0 nm was scanned at 200 nm/s.

To provide a deeper understanding of the behavior of the nanoporous HOPG surfaces, we studied and compared the electrochemical properties of the HOPG and nanoporous HOPG electrodes by Electrochemical Impedance Spectroscopy (EIS). Figure 4A shows EIS results using ferricyanide as an electrochemical probe. Both electrodes present the characteristic semicircle in the Nyquist representation with a sinusoidal wave. The resistance to charge transfer values calculated from the diameter were 160 Ω and 80 Ω for HOPG and nanoporous HOPG, respectively. Hence, the nanoporous surface of HOPG is much more conductive than the exfoliated HOPG. These results are in agreement with the results obtained by other authors with porous carbon structures [6, 15].

From chronoamperometry measurements applying the Cottrell Eq. (2) and using ferricyanide as the redox probe, the electroactive area of several nanoporous HOPG electrodes was calculated.

$$i = \frac{nFA\sqrt{D_0C_0}}{\sqrt{\pi t}} \quad (2)$$

where n is the number of electrons involved in the reaction, F is the Faraday's constant, C_0 and D_0 are the bulk concentration and diffusion coefficient of the redox probe, t is the time. It was found to be (0.50 ± 0.01) cm² ($n = 3$), which in comparison with the geometric area of the surface exposed to the solution (0.12 cm²) represents an increase of 3.5 times. This is in accordance with the results shown above, since there has been an increase in electrode

reactivity due to the increase in sp^3 carbons. The capacitive current of the HOPG electrode is also significantly higher when it comes to a nanoporous HOPG electrode compared to flat HOPG (Fig. SI 6).

Deepening inside the carbon structure, Raman spectroscopy is a technique widely employed to carbon surfaces characterization. Thus, Fig. 4B shows the Raman spectra of both freshly exfoliated and nanoporous HOPG surfaces, observing in both cases the characteristic bands of carbon [32]: D-band and G-band at 1355 and 1580 cm^{-1} respectively, G' band (also denoted in bibliography as 2D) at 2800 cm^{-1} and a small band at 2450 cm^{-1} , denoted as G* and related to other overtones of D-band [33]. The main difference between the spectra is the D-band displayed in the nanoporous HOPG, which is associated to sp^2 hybridization and is distinctive of the present of defects with partially messy structures on the graphite surface [34, 35]. This band is absent in the exfoliated HOPG surface spectrum, since it is free of defects.

These results confirm that more reactive areas have been generated, mainly associated with edge planes, due to the presence of holes in the surface of a perfectly exfoliated electrode.

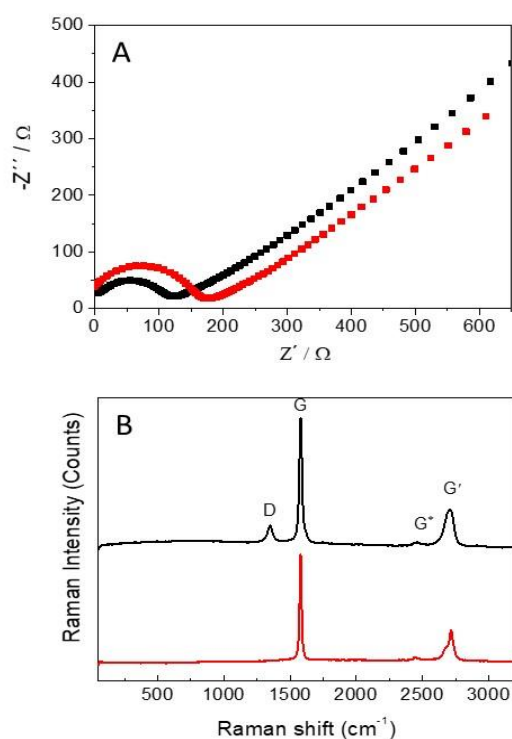


Figure 4. A) The electrochemical impedance spectroscopy (EIS) represented as a Nyquist plot of exfoliated (red square) and nanoporous HOPG electrode (black square) in 1.0 mM $K_4[Fe(CN)_6]$ in 0.1 M phosphate buffer pH 7.4 containing 0.05 M KCl. B) Raman spectra of exfoliated (red line) and nanoporous (black line) HOPG electrode.

As has been demonstrated throughout this experimental work, a nanoporous structure has been generated on the HOPG surface. As mentioned in the introduction, materials with these characteristics are very attractive in electrochemistry for energy storage, specifically as supercapacitor. Galvanostatic charge-discharge experiments and cyclic voltammetry studies have been performed in order to evaluate the potential application of nanoporous HOPG as supercapacitor (Fig. 5). Both kinds of measurements have been

carried out in 1 M H_2SO_4 solution using a two electrodes configuration. Typically, the capacitance of the supercapacitor is evaluated from the charge/discharge cycles slope, using Eq. (3):

$$C_{Total} = \frac{I}{2 \times \left(\frac{dV}{dt}\right) \times A} \quad (3)$$

where I is the current applied, V is the potential measured over time (t) and A is the electrode geometric area. Fig. 5A shows the charge-discharge curves of nanoporous HOPG and the control exfoliated HOPG at 100 nA of current. As can be observed, the lineal region presents a higher slope in the case of HOPG compared with nanoporous HOPG, which demonstrates the increase of capacitance in nanoporous HOPG.

Figure 5B shows the capacitances calculated from the different charge-discharge measurements, fixing different currents. Similar results were obtained by cyclic voltammetry as is shown in Figure 5C. Fig. 5D shows the voltammograms between 1.00 and -1.00 V, of two nanoporous HOPG electrodes (black curve) and also the CV of two exfoliated HOPG (red curve). The capacitance of the working electrode was calculated from the corresponding voltammograms, using the following Eq. (4):

$$C_{Total} = \frac{\int_{V_1}^{V_2} I(V) dV}{2 \times \Delta V \times \nu \times A} \quad (4)$$

where C_{Total} is the specific capacitance exhibited by the working electrode in $\mu F/cm^2$, $\int I(V) dV$ is the area under the intensity current function between V_2 and V_1 potentials in Coulombs (C), ΔV is the potential difference between V_2 and V_1 in volts (V), ν is the voltammogram scan rate in volts per second (V/s) and A is the electrode geometric area. The capacitance obtained by cyclic voltammetry experiments (Fig. 5D) shows similar values to those obtained by galvanostatic charge-discharge experiments. As can be observed in the minimum current, nanoporous HOPG shows a specific capacitance close to 160 $\mu F/cm^2$ while the capacitance at the same current for HOPG is around 6 $\mu F/cm^2$. It is remarkable that the creation of nanopores on the HOPG surface results in an increase of more than 25 times the material capacitance. This fact highlights the great increase of electroactive area after the nanopores generation, which highly increases the energy storage in the double layer of the electrodes system. It is worth to point out that this huge increase is reached only changing the nanoporosity of the material under study and not by the modification with other expensive materials or redox species.

Long-term cycling stability of electrode material is a requirement for practical application. The nanoporous HOPG showed more than 5000 cycle stability. The capacitance lost after 5000 cycles was of 89.8 % (Fig. SI 7).

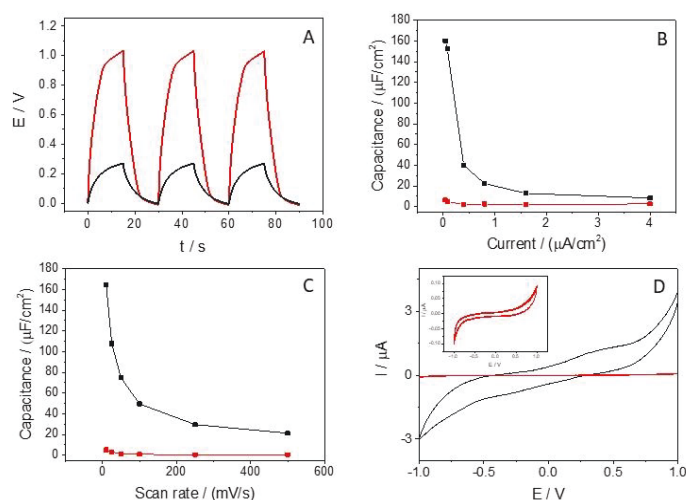


Figure 5. A) Charge/discharge curves of a HOPG (red line) and nanoporous HOPG (black line) electrode-based supercapacitor applying a current of $0.8 \mu\text{A}/\text{cm}^2$ in 1 M H_2SO_4 using a two electrodes configuration. B) Current and C) Scan rate response of the capacitance of a HOPG (red line) and nanoporous HOPG (black line) electrode-based supercapacitor. D) Cyclic voltammograms of exfoliated (red line) and nanoporous (black line) HOPG electrode at 10 mV/s scan rate in 1 M H_2SO_4 using a two electrodes configuration.

4 Conclusions

A new method for preparing nanoporous HOPG surfaces, without the need of hard conditions has been developed. CND combined with the electrochemical etching treatment are the responsible of generating nanopores on the HOPG surface. The pore size can be controlled by the number of voltammetric cycles applied. The nanoporous surface has been characterized by AFM, SECM, EIS and Raman, which has allowed to demonstrate that the presence of nanopores significantly increases the reactivity of the surface in addition to the area. The development of these nanoporous surfaces is of great interest in applications such as energy storage and catalysis, among others. As proof of concept, the nanoporous HOPG developed has been applied to the fabrication of supercapacitor in a two electrodes configuration.

Acknowledgements

The authors grateful thank Professor H. D. Abruña from Cornell University the critical review of this work. The authors are grateful for the financial support provided by the Ministerio de Ciencia, Innovación, Universidades of Spain (CTQ2017-84309-C2-1-R; RED2018-102412-T), Comunidad Autónoma de Madrid (TRANSNANOAVANSENS Program) and Generalitat Valenciana (APOSTD/2017/010). C. G-S. also acknowledges the financial support from the Comunidad Autónoma de Madrid, Atracción de Talento Program (2017-T1/BIO-5435).

Electronic Supplementary Material: Supplementary material is available in the online version of this article at http://dx.doi.org/10.1007/s12274-***-****- (automatically inserted by the publisher with additional experimental details of the AFM, SECM measurements and electrochemical characterization are available.

References

- [1] Rajagopalan, R.; Ponnaiyan, A.; Mankidy, P. J.; Brooks, A. W.; Yi, B.; Foley, H. C. Molecular sieving platinum nanoparticle catalysts kinetically frozen in nanoporous carbon. *Chemical Communications* **2004**, 10.1039/b407854c, 2498-2499.
- [2] Hauser, A. W.; Schwerdtfeger, P. Nanoporous Graphene Membranes for Efficient $3\text{He}/4\text{He}$ Separation. *The Journal of Physical Chemistry Letters* **2012**, 3, 209-213.
- [3] Han, T. H.; Huang, Y.-K.; Tan, A. T. L.; Dravid, V. P.; Huang, J. Steam Etched Porous Graphene Oxide Network for Chemical Sensing. *Journal of the American Chemical Society* **2011**, 133, 15264-15267.
- [4] Soni, R.; Bhange, S. N.; Kurungot, S. A 3-D nanoribbon-like Pt-free oxygen reduction reaction electrocatalyst derived from waste leather for anion exchange membrane fuel cells and zinc-air batteries. *Nanoscale* **2019**, 11, 7893-7902.
- [5] Mo, R.; Li, F.; Tan, X.; Xu, P.; Tao, R.; Shen, G.; Lu, X.; Liu, F.; Shen, L.; Xu, B.; Xiao, Q.; Wang, X.; Wang, C.; Li, J.; Wang, G.; Lu, Y. High-quality mesoporous graphene particles as high-energy and fast-charging anodes for lithium-ion batteries. *Nature Communications* **2019**, 10, 1474.
- [6] Han, S.; Wu, D.; Li, S.; Zhang, F.; Feng, X. Porous Graphene Materials for Advanced Electrochemical Energy Storage and Conversion Devices. *Advanced Materials* **2014**, 26, 849-864.
- [7] Khiari, B.; Jeguirim, M.; Limousy, L.; Bennici, S. Biomass derived chars for energy applications. *Renewable and Sustainable Energy Reviews* **2019**, 108, 253-273.
- [8] Hui, F.; Li, B.; He, P.; Hu, J.; Fang, Y. Electrochemical fabrication of nanoporous polypyrrole film on HOPG using nanobubbles as templates. *Electrochemistry Communications* **2009**, 11, 639-642.
- [9] Hugentobler, M.; Bonanni, S.; Sautier, A.; Harbich, W. Morphology and stability of Au nanoclusters in HOPG nanopits of well-defined depth. *The European Physical Journal D* **2011**, 63, 215-220.
- [10] Stankovich, S.; Dikin, D. A.; Dommett, G. H. B.; Kohlhaas, K. M.; Zimney, E. J.; Stach, E. A.; Piner, R. D.; Nguyen, S. T.; Ruoff, R. S. Graphene-based composite materials. *Nature* **2006**, 442, 282-286.
- [11] Jana, D.; Vasista, A. B.; Jog, H.; Tripathi, R. P. N.; Allen, M.; Allen, J.; Pavan Kumar, G. V. V-shaped active plasmonic meta-polymers. *Nanoscale* **2019**, 11, 3799-3803.
- [12] Shen, A.; Zou, Y.; Wang, Q.; Dryfe, R. A. W.; Huang, X.; Dou, S.; Dai, L.; Wang, S. Oxygen Reduction Reaction in a Droplet on Graphite: Direct Evidence that the Edge Is More Active than the Basal Plane. *Angewandte Chemie International Edition* **2014**, 53, 10804-10808.
- [13] Kurra, N.; Prakash, G.; Basavaraja, S.; Fisher, T. S.; Kulkarni, G. U.; Reifengerger, R. G. Charge storage in mesoscopic graphitic islands fabricated using AFM bias lithography. *Nanotechnology* **2011**, 22, 245302.
- [14] Corgier, B. P.; Bélanger, D. Electrochemical Surface Nanopatterning Using Microspheres and Aryldiazonium. *Langmuir* **2010**, 26, 5991-5997.
- [15] Cui, L.; Xu, Y.; Liu, B.; Yang, W.; Song, Z.; Liu, J. Well-controlled preparation of evenly distributed nanoporous HOPG surface via diazonium salt assisted electrochemical etching process. *Carbon* **2016**, 102, 419-425.
- [16] Phan, T. H.; Van Gorp, H.; Li, Z.; Trung Huynh, T. M.; Fujita, Y.; Verstraete, L.; Eyley, S.; Thielemans, W.; Uji-i, H.; Hirsch, B. E.; Mertens, S. F. L.; Greenwood, J.; Ivasenko, O.; De Feyter, S. Graphite and Graphene Fairy Circles: A Bottom-Up Approach for the Formation of Nanocorrals. *ACS Nano* **2019**, 13, 5559-5571.
- [17] Xu, X.; Ray, R.; Gu, Y.; Ploehn, H. J.; Gearheart, L.; Raker, K.; Scrivens, W. A. Electrophoretic Analysis and Purification of Fluorescent Single-Walled Carbon Nanotube Fragments. *Journal of the American Chemical Society* **2004**, 126, 12736-12737.
- [18] Rigodanza, F.; Đorđević, L.; Arcudi, F.; Prato, M. Customizing the Electrochemical Properties of Carbon Nanodots by Using Quinones in Bottom-Up Synthesis. *Angewandte Chemie International Edition* **2018**, 57, 5062-5067.
- [19] Gutiérrez-Sánchez, C.; Mediavilla, M.; Guerrero-Esteban, T.; Revenga-Parra, M.; Pariente, F.; Lorenzo, E. Direct covalent immobilization of new nitrogen-doped carbon nanodots by electrografting for sensing applications. *Carbon* **2020**, 159, 303-310.

- [20] Abad, J. M.; Tesio, Á. Y.; Pariente, F.; Lorenzo, E. Patterning Gold Nanoparticle Using Scanning Electrochemical Microscopy. *The Journal of Physical Chemistry C* **2013**, *117*, 22087-22093.
- [21] Abad, J. M.; Tesio, A. Y.; Martínez-Periñán, E.; Pariente, F.; Lorenzo, E. Imaging resolution of biocatalytic activity using nanoscale scanning electrochemical microscopy. *Nano Research* **2018**, *11*, 4232-4244.
- [22] Wang, Y.; Limon-Petersen, J. G.; Compton, R. G. Measurement of the diffusion coefficients of $[\text{Ru}(\text{NH}_3)_6]^{3+}$ and $[\text{Ru}(\text{NH}_3)_6]^{2+}$ in aqueous solution using microelectrode double potential step chronoamperometry. *Journal of Electroanalytical Chemistry* **2011**, *652*, 13-17.
- [23] Nioradze, N.; Chen, R.; Kim, J.; Shen, M.; Santhosh, P.; Amemiya, S. Origins of Nanoscale Damage to Glass-Sealed Platinum Electrodes with Submicrometer and Nanometer Size. *Analytical Chemistry* **2013**, *85*, 6198-6202.
- [24] Yuan, W.; Zhou, Y.; Li, Y.; Li, C.; Peng, H.; Zhang, J.; Liu, Z.; Dai, L.; Shi, G. The edge- and basal-plane-specific electrochemistry of a single-layer graphene sheet. *Scientific Reports* **2013**, *3*, 2248.
- [25] Zoval, J. V.; Lee, J.; Gorer, S.; Penner, R. M. Electrochemical Preparation of Platinum Nanocrystallites with Size Selectivity on Basal Plane Oriented Graphite Surfaces. *The Journal of Physical Chemistry B* **1998**, *102*, 1166-1175.
- [26] Lu, J.; Yang, J.-x.; Wang, J.; Lim, A.; Wang, S.; Loh, K. P. One-Pot Synthesis of Fluorescent Carbon Nanoribbons, Nanoparticles, and Graphene by the Exfoliation of Graphite in Ionic Liquids. *ACS Nano* **2009**, *3*, 2367-2375.
- [27] Jurewicz, K.; Frackowiak, E.; Béguin, F. Towards the mechanism of electrochemical hydrogen storage in nanostructured carbon materials. *Applied Physics A* **2004**, *78*, 981-987.
- [28] Morales, G. M.; Schifani, P.; Ellis, G.; Ballesteros, C.; Martínez, G.; Barbero, C.; Salavagione, H. J. High-quality few layer graphene produced by electrochemical intercalation and microwave-assisted expansion of graphite. *Carbon* **2011**, *49*, 2809-2816.
- [29] Robinson, R. S. Morphology and Electrochemical Effects of Defects on Highly Oriented Pyrolytic Graphite. *Journal of The Electrochemical Society* **1991**, *138*, 2412.
- [30] McDermott, M. T.; Kneten, K.; McCreery, R. L. Anthraquinonedisulfonate adsorption, electron-transfer kinetics, and capacitance on ordered graphite electrodes: the important role of surface defects. *The Journal of Physical Chemistry* **1992**, *96*, 3124-3130.
- [31] Sun, T.; Yu, Y.; Zacher, B. J.; Mirkin, M. V. Scanning Electrochemical Microscopy of Individual Catalytic Nanoparticles. *Angewandte Chemie International Edition* **2014**, *53*, 14120-14123.
- [32] Malard, L. M.; Pimenta, M. A.; Dresselhaus, G.; Dresselhaus, M. S. Raman spectroscopy in graphene. *Physics Reports* **2009**, *473*, 51-87.
- [33] Sokolov, A. P.; Buchenau, U.; Steffen, W.; Frick, B.; Wischnewski, A. Comparison of Raman- and neutron-scattering data for glass-forming systems. *Physical Review B* **1995**, *52*, R9815-R9818.
- [34] Suk, J. W.; Kitt, A.; Magnuson, C. W.; Hao, Y.; Ahmed, S.; An, J.; Swan, A. K.; Goldberg, B. B.; Ruoff, R. S. Transfer of CVD-Grown Monolayer Graphene onto Arbitrary Substrates. *ACS Nano* **2011**, *5*, 6916-6924.
- [35] Solís-Fernández, P.; Paredes, J. I.; Cosío, A.; Martínez-Alonso, A.; Tascón, J. M. D. A comparison between physically and chemically driven etching in the oxidation of graphite surfaces. *Journal of Colloid and Interface Science* **2010**, *344*, 451-459.

Carbon nanodots: a new precursor to achieve reactive nanoporous HOPG surfaces

C. Gutiérrez-Sánchez ¹ (✉), E. Martínez-Periñán ¹, C. Busó-Rogero ³, M. Revenga-Parra ^{1,2,3}, F. Pariente ^{1,2}, E. Lorenzo ^{1,2,3} (✉)

¹ Departamento de Química Analítica y Análisis Instrumental and ² Institute for Advanced Research in Chemical Sciences (IAdChem), Universidad Autónoma de Madrid, Campus de Cantoblanco, 28049 Madrid, Spain.

³ IMDEA-Nanoscience. Faraday 9, Campus Cantoblanco-UAM, 28049 Madrid, Spain.

© Tsinghua University Press and Springer-Verlag GmbH Germany, part of Springer Nature 2018

Received: day month year / **Revised:** day month year / **Accepted:** day month year (automatically inserted by the publisher)

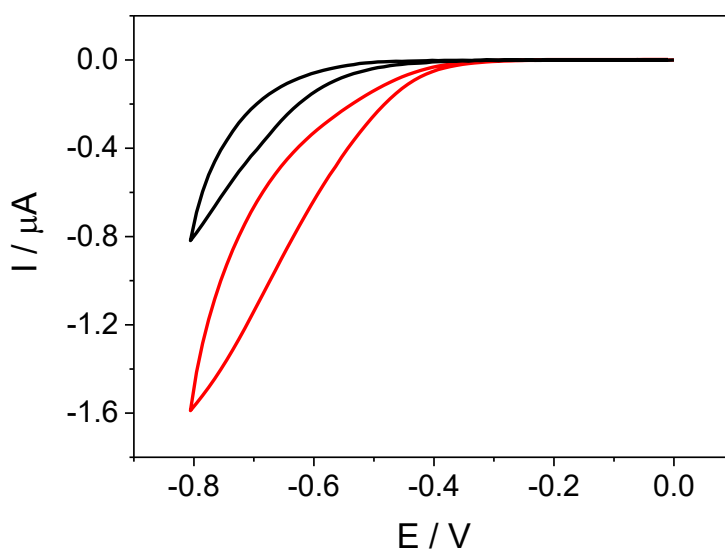


Figure SI 1. Cyclic voltammograms of an exfoliated HOPG electrode immersed in a solution of CND in 0.1 M HCl (red line) and in 0.1 M HCl without CND (black line). Scan rate: 100 mV/s.

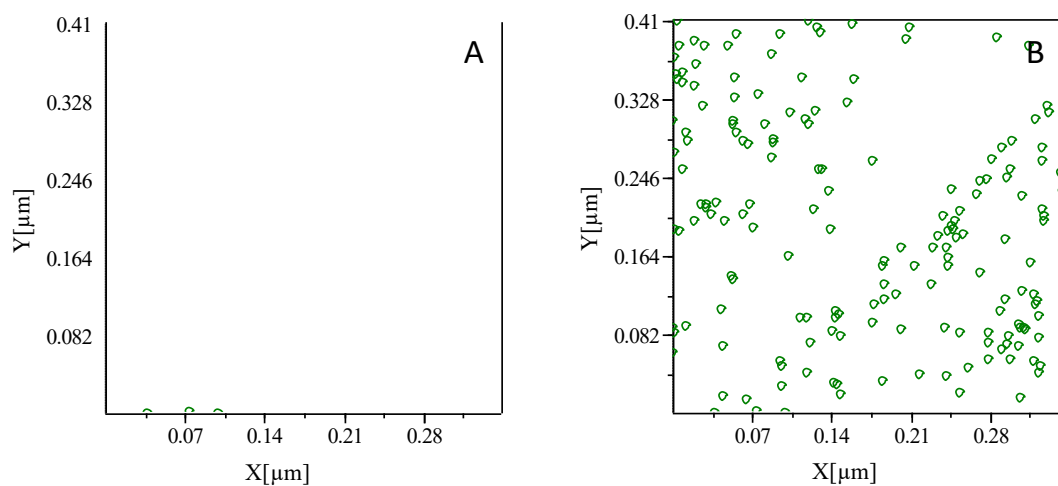


Figure SI 2. Center map of nanoporous on exfoliated HOPG from Figure 1A (A) and nanoporous HOPG (50 cycles) from Figure 1C (B).

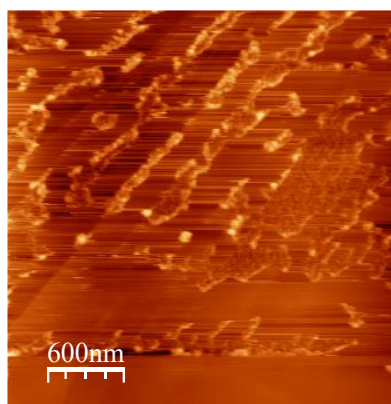


Figure SI 3. AFM image of HOPG electrode after being treated with more than 100 voltammetric cycles in 0.1 M HCl in the presence of CND.

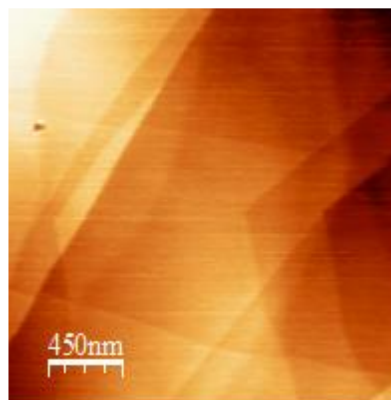


Figure SI 4. AFM image of HOPG electrode after being treated with 10 voltammetric cycles in 0.1 M HCl in the absence of CND.

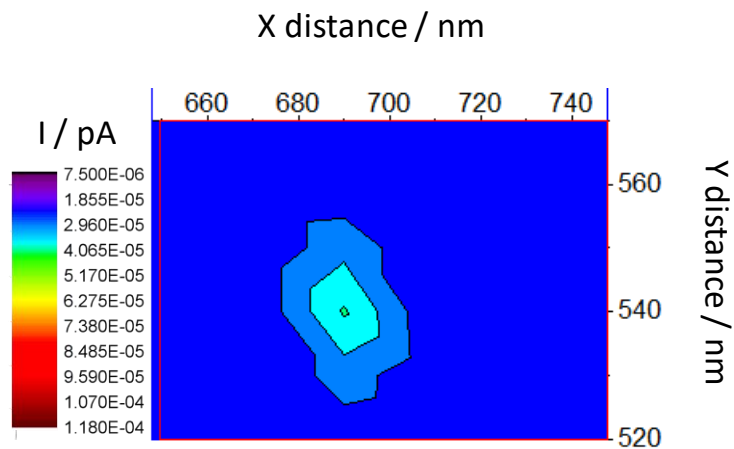


Figure SI 5. SECM mapping of an individual nanopore. The measurement was obtained with 1.0 mM $[\text{Ru}(\text{NH}_3)_6]^{3+}$ in 0.1 M KCl at $E_{\text{tip}} = +0.10$ V and $E_{\text{substrate}} = -0.40$ V vs. Ag/AgCl. Pt. Nanotip was scanned at 200 nm/s.

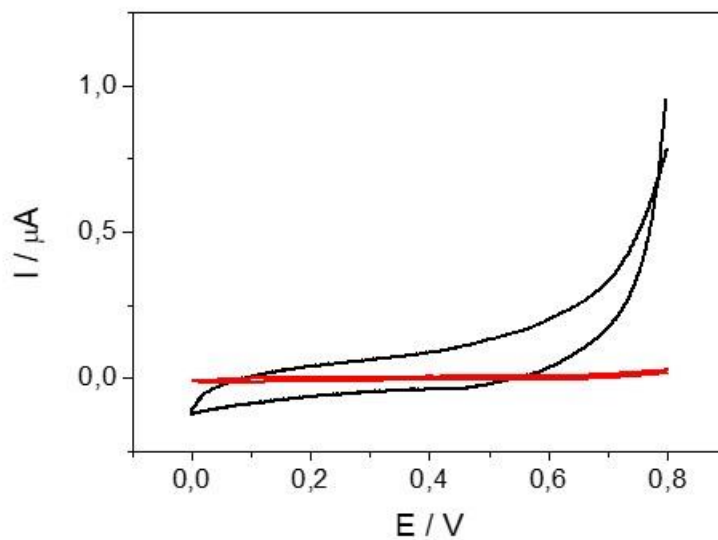


Figure SI 6. Cyclic voltammograms of exfoliated (red line) and nanoporous (black line) HOPG electrode at 100 mV/s scan rate in 0.1 M phosphate buffer pH 7.4.

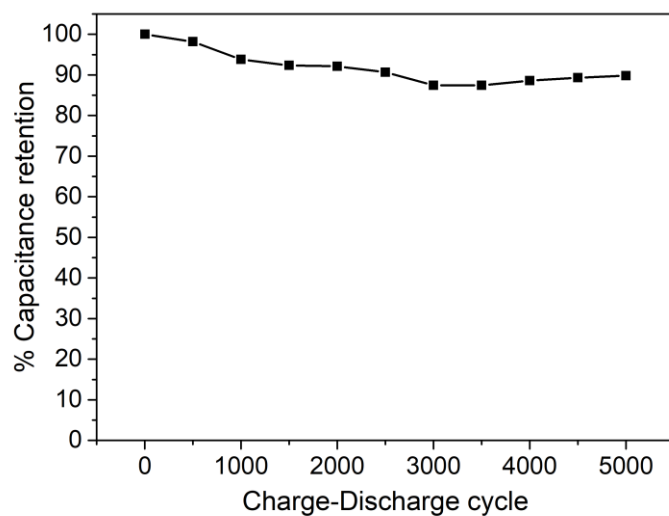


Figure SI 7. Relative capacitance for successive charge–discharge cycles respect the first cycle capacitance for two nanoporous HOPG plates immersed in 0.5 M H₂SO₄.

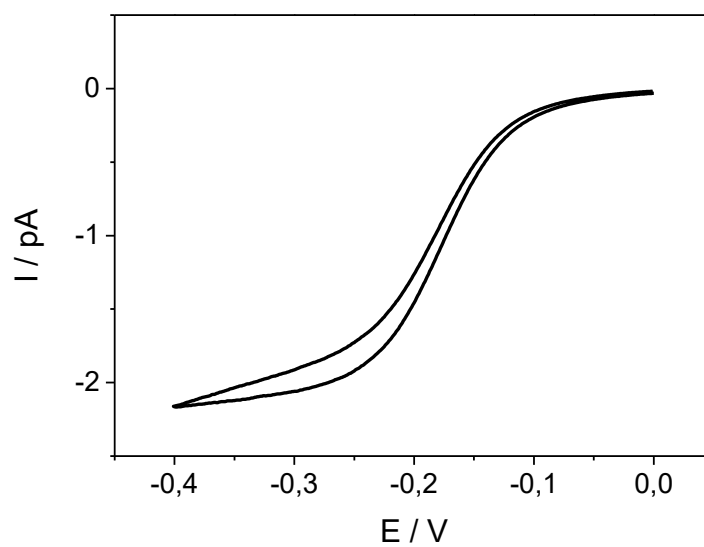


Figure SI 8. Cyclic voltammetry of Pt tip UME at 1.0 mM [Ru(NH₃)₆]³⁺ in 0.1 M KCl.

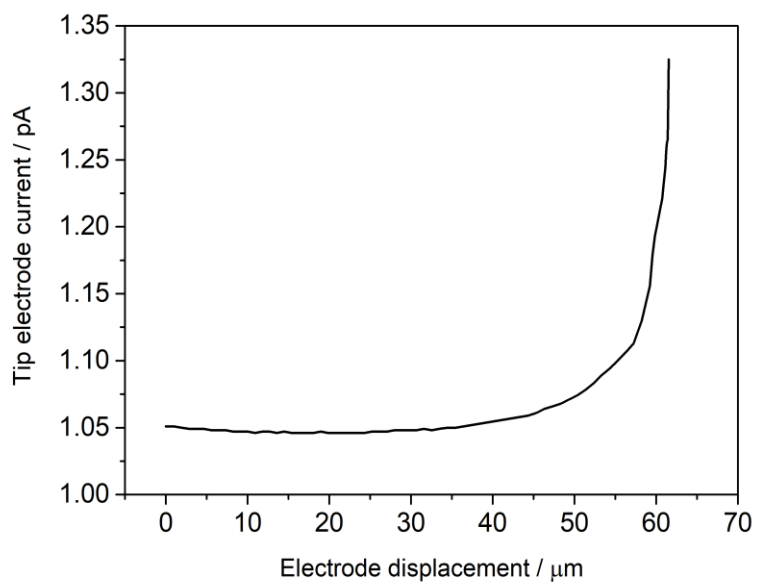


Figure SI 9. Approach curve for a nanoporous HOPG surface via electrochemical reduction of 1.0 mM $[\text{Ru}(\text{NH}_3)_6]^{3+}$ in 0.1 M KCl, when a potential of -0.40 V was applied at the tip, and the surface was kept unbiased.